The Astrophysical Journal, 891:54 (8pp), 2020 March 1 https://doi.org/10.3847/1538-4357/ab6f6c

Peak Temperatures of Large Solar X-Ray Flares and Associated CME Speeds and Widths

A. G. Ling[1] and S. W. Kahler[2]
[1] Atmospheric Environmental Research, Albuquerque, New Mexico 87110, USA; ALing@aer.com
[2] Air Force Research Laboratory, Space Vehicles Directorate, 3550 Aberdeen Avenue, Kirtland AFB, NM 87117, USA
Received 2019 September 26; revised 2020 January 14; accepted 2020 January 22; published 2020 March 3

Abstract

We recently repeated an earlier analysis by Garcia showing that large (≥M3.0) solar X-ray flares associated with solar energetic particle (SEP) events have significantly lower peak X-ray flux ratios $R = (0.04–0.5\,\mathrm{nm})/(0.1–0.8\,\mathrm{nm})$, proxies for flare peak temperatures, than those without SEP events. As we expect SEP events to be produced by shocks ahead of fast coronal mass ejections (CMEs), a smaller R for an X-ray flare of a given peak flux Fp should also be more likely to be accompanied by a fast ($V\mathrm{cme} > 1000\,\mathrm{km\,s^{-1}}$) CME. We confirm this expectation, examine the role played by the ratios R in correlations between Fp and CME speeds Vcme, and then compare CME widths W, Vcme, and R with each other. We consider an apparent conflict between a global scaling model of eruptive events showing Vcme scaling with higher R and our confirmation that the Garcia analysis implies that faster CMEs are associated with flares of lower R. The R values are examined for 16 large flares of the well-studied AR 12192, for which nearly all flares had no associated CMEs. Those flares share the same high values of R as other active region (AR) flares with no CMEs. We also find that small (<M3.0) flares of filament eruptions leading to SEP events share the lower R values of larger flares with fast CMEs.

Unified Astronomy Thesaurus concepts: Solar flares (1496); Solar coronal mass ejections (310); Solar coronal mass ejection shocks (1997); Solar x-ray flares (1816); Solar flare spectra (1982); Solar active regions (1974)

Supporting material: machine-readable table

1. Introduction

Large solar energetic ($E > 10\,\mathrm{MeV}$) particle (SEP) events are understood to be produced in coronal shocks driven by fast ($V\mathrm{cme} \geqslant 900\,\mathrm{km\,s^{-1}}$) coronal mass ejections (CMEs; Reames 2013, 2017, 2018; Desai & Giacalone 2016). Those CMEs are nearly always accompanied by solar X-ray flares observed in the 0.1–0.8 nm band of the *GOES* X-ray Spectrometer (XRS), which are commonly used to forecast the occurrence of SEP events (Balch 2008; Belov 2009; Kahler et al. 2017; Nuñez 2018). Garcia (1994, 2004) took a novel approach to comparing *GOES* X-ray observations with SEP events by introducing the peak flare X-ray temperatures, T_e, based on the ratios of short (0.05–0.4 nm) to long (0.1–0.8 nm) wavelength bands. The flare temperatures were based on an isothermal source assumption and a model thermal spectrum matched to the detector passbands. For a given range of peak 0.1–0.8 nm flare fluxes, Fp, the SEP events were preferentially associated with flares of lower peak temperatures.

Recently, we (Kahler & Ling 2018, hereafter KL18) revisited the Garcia approach using a compilation of all ≥M3.0 X-ray flares with known source locations from 1998 to 2016. Rather than flare temperatures, we used simply the background-corrected peak flare ratios R of short (0.05–0.4 nm) to long (0.1–0.8 nm) wavelength fluxes, which scale non-linearly with the modeled temperature Te. We plotted R versus the 0.1–0.8 nm peak fluxes Fp (in a log–log format (hereafter *R–Fp* plots)) to sort out flare groups with (1) no associated SEP event; (2) a small (1.2–9.9 pfu (proton flux unit = 1 p $\mathrm{cm^{-2}\,sr^{-1}\,s^{-1}}$ above 10 MeV) event; (3) a NOAA Space Weather Prediction Center (SWPC) (≥10 pfu) event (ftp.swpc.noaa.gov/pub/indices/SPE.txt); or (4) a ⩾ 300 pfu event. The flares were divided into east and west hemisphere groups and plotted separately as shown in the left panels of Figure 1, a modified version of the KL18 Figure 5. KL18 used the statistical t-test (Wilks 2006) to calculate probabilities P that the SEP events and non-SEP events were drawn from a common population for three selected bins of R. Their P values (reproduced in Table 1) were $\leqslant 6.2 \times 10^{-3}$ for each bin, statistically validating their and Garcia (1994, 2004)) findings of clear separations between the SEP and non-SEP groups based on R. We want to determine whether other particular population pairs are significantly separated from each other and will also use the t-test probabilities P as guides to our results.

The introduction of peak-flux ratios R adds information to any X-ray flare-based scheme to forecast SEP events, but it challenges our understanding of the physics behind the basic result of Figure 1 left panels. The current paradigm of SEP origins in CME-driven shocks is validated by the many results of good correlations between SEP peak intensities Ip and associated CME speeds Vcme (Reames 2013, 2017; Belov 2017; Park et al. 2017). However, correlations of SEP Ip versus flare Fp tend to match those of SEP Ip versus Vcme (Cane et al. 2010; Miteva et al. 2013; Park & Moon 2014; Dierckxsens et al. 2015; Valtonen & Ameri 2015; Takahashi et al. 2016), suggesting that flares are somehow equally important as CMEs in driving SEP events.

The question now is whether lower-temperature X-ray flares are physically connected with the faster CMEs needed for SEP production. KL18 pointed out that a global analysis by Aschwanden (2017) of 860 *GOES* M and X-class solar flares and associated CMEs led to a scaling law of $V\mathrm{cme} \sim T_e^{0.5}$, a result seemingly in conflict with our results. The correlation between Fp and associated CME Vcme (Yashiro & Gopalswamy 2008; Salas-Matamoros & Klein 2015) shows a clear connection between flares and CMEs, but any role for flare temperatures Te is not included in those correlations.

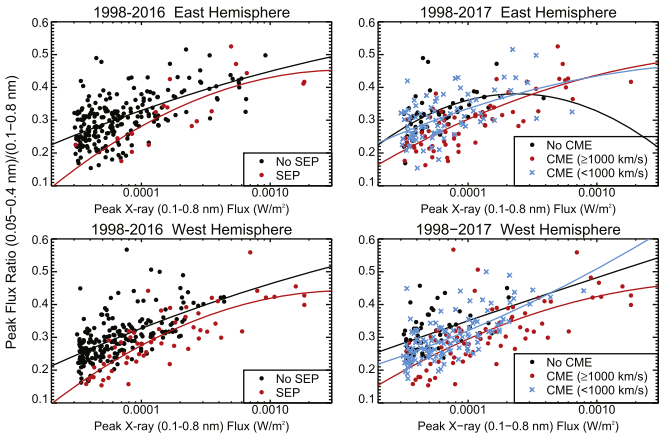

Figure 1. Left panels: modified version of Figure 5 of KL18, following their *R–Fp* format. Top left: *R–Fp* plot for 247 NOAA flares in the east hemisphere. Bottom left: same for 261 NOAA flares in the west hemisphere. Solid lines are polynomial quadratic best fits to the No-SEP and SEP populations. Right panels: *R–Fp* plot for three classes of *V*cme associations of 200 east hemisphere flares (top) and 250 west hemisphere flares (bottom) updated through 2017. Solid lines are least-squares quadratic fits to color-matched symbols.

Accepting the CME-shock paradigm for SEP events, the clear implication of Figure 1 is that a similar plot format discriminating among (1) faster SEP-producing CMEs; (2) slower non-SEP-producing CMEs; and (3) no CMEs should yield a result similar to that with SEP and non-SEP events. Here, we use *R–Fp* plots to test that implication for CME speeds *V*cme.

2. Data Analysis

2.1. Peak-flux Ratios and CME Speeds

Our goal is to determine whether the *R–Fp* format of Figure 1 also sorts CME speeds as it does SEP events. We begin with the same KL18 list of all *GOES*/XRS ⩾ M3.0 flares with given flare locations from 1998 to 2016 taken from ftp.ngdc.noaa.gov. There were 433 flares without and 75 flares with ⩾10 pfu SEP events in that list. We changed the flare locations of four events and added five events from 2014 October, originally excluded due to lack of flare locations, to make a total of 513 flare events. We then added 16 additional flares in 2017 from ftp.swpc.noaa.gov, bringing the new total to 529. As in KL18, we consider separately the eastern and western hemisphere flares.

The timing and location of each X-ray flare was compared with CMEs reported on the *Solar and Heliospheric Observatory* (*SOHO*)/ Large Angle and Spectromeric Coronagraph Experiment (LASCO) website (https://cdaw.gsfc.nasa.gov/CME_list/index.html) to determine the CME association, if any, for each flare. LASCO data gaps during 51 flares reduced the comparisons to a total of 478 cases, which were then compared with the CME-flare associations at https://cdaw.gsfc.nasa.gov/pub/yashiro/flare_cme/fclist_pub.txt (hereafter fclist; Yashiro et al. 2006, 2008). The fclist includes all *GOES*/XRS ⩾ M1 flares with associated flare locations and draws on the CME values reported in the *SOHO*/LASCO website. The various association discrepancies between the two lists were resolved, nearly all in accord with those of the fclist, reducing the total to 450 events, of which we differ from the fclist in only 11 cases. The 450 event associations are listed in Table 3. The first five columns give the date, peak time, size, location, and *R* for each flare. The CME linear speed *V*cme in km s^{-1} and width *W* in angular degrees of each associated CME is given in columns 6 and 7. The 52 eastern hemisphere and 60 western hemisphere flares with no associated CMEs ("none") are included in Table 3.

For future reference we add onset dates, times and peak intensities *Ip* of any associated SEP events as reported in Table 1 of Kahler & Ling (2019a, hereafter KL19a). Note that some of their SEP events had no associated ⩾M3.0 flares and are not included in our Table 3. We also made the following corrections to the KL19a Table 1: (1) 2002 April 21, change *Ip* from 350 to 3500 pfu; (2) 2013 January 17, change N20E87 to S32W87; (3) 2013 November 19, change S70W14 to S13W69; and (4) add an SEP event at 2003 June 18/0900 (details in our Table 3). We regret the errors. Finally, a preliminary version of this work is given in Kahler & Ling (2019b, hereafter KL19b).

In the right panels of Figure 1, we plot the 450 CME associations using the *R–Fp* format matching the left panels, now dividing the CME associations into three groups of (1) no, (2) slow (*V*cme < 1000 km s^{-1}), and (3) fast (*V*cme ⩾ 1000 km s^{-1}) CMEs. As perhaps expected from the SEP results of the left panels, the fast CMEs lie preferentially in the low range of the *R* ratios. The no-CME and slow-CME groups are not so well separated, as the least-squares fits of the plots indicate.

Table 1 gives the t-test probabilities *P* of common source populations among the three groups. Following the results of KL18, we first divide the populations of each panel into separate groups with fixed ranges of *R*, rather than of *Fp*. In the top section of Table 1 we repeat the t-test results of KL18 comparing the no-SEP flares with the SEP flares of Figure 1 in low, medium, and high ranges of *R*, defined by requiring approximately equal numbers of events in each range of *R*. With smaller numbers of events in each of the three CME groups than in the two SEP groups, we divided the peak-flux ratio *R* into only two ranges at $R = 0.307$ for the East Hemisphere and 0.300 for the West Hemisphere. The no-CME groups are well separated from the fast CMEs, with $P < 9.5 \times 10^{-3}$ for both *R* bins in both hemispheres. We test only the no CMEs versus slow CMEs and the slow CMEs versus fast-CMEs groups, shown in the middle part of Table 1. For the CME speed groups of Figure 1 we find only modest ($P \sim 4.5 \times 10^{-3}$ to 1.8×10^{-1}) values comparing the no-CME with slow-CME groups, but much lower ($P < 3 \times 10^{-3}$ for all but one bin) values distinguishing the slow and fast CME groups. This result validates the suspected reason for the SEP and no-SEP separation of Figure 1, that the SEP events result from associations with fast (*V*cme ⩾ 1000 km s^{-1}) CMEs rather than flares with no or slow CMEs.

Statistical correlations between X-ray *Fp* and associated CME *V*cme have been found in several studies with (Miteva et al. 2013; Trottet et al. 2015) and without associated SEP events (Yashiro & Gopalswamy 2008; Salas-Matamoros & Klein 2015), and we now ask whether the *R* ratios show any systematic variations within those correlations. As noted in KL18 and shown in Figure 1, there is a general increase of *R* with *Fp*. Figure 2 shows log–log plots of *Fp* versus *V*cme for flares in each hemisphere, again separated into three bands of *R*, where the bands are chosen to yield approximately the same number of flares in each *R* group. Flares with no CMEs are plotted at log *V*cme = 2.0. As we do not want to specify which is the independent variable, we show in

Table 1
t-test Distribution Differences Between Groups of Events

Hemisphere	Peak-flux Ratio R	P[a]	t	SEP/Vcme/Flare Comparison Groups
Eastern	<0.27	1.6 E−4	3.97	No-SEP versus SEPs (KL18)
	0.27–0.33	6.2 E−3	2.81	No-SEP versus SEPs (KL18)
	>0.33	9.7 E−7	5.30	No-SEP versus SEPs (KL18)
Western	<0.26	2.0 E−5	4.51	No-SEP versus SEPs (KL18)
	0.26–0.32	4.5 E−6	4.90	No-SEP versus SEPs (KL18)
	>0.32	1.7 E−8	6.24	No-SEP versus SEPs (KL18)
Eastern	<0.31	1.0 E−1	1.67	No-CME versus Vcme (<1000 km s^{-1})
	<0.31	2.5 E−1	1.16	Vcme (⩾1000 km s^{-1}) versus Vcme (<1000 km s^{-1})
	⩾0.31	1.8 E−1	1.34	No-CME versus Vcme (<1000 km s)
	⩾0.31	2.7 E−3	3.13	Vcme (⩾1000 km s^{-1}) versus Vcme (<1000 km s^{-1})
Western	<0.30	1.5 E−2	2.48	No-CME versus Vcme (<1000 km s^{-1})
	<0.30	4.8 E−5	4.26	Vcme (⩾1000 km s^{-1}) versus Vcme (<1000 km/s^{-1})
	⩾0.30	4.5 E−3	2.93	No-CME versus Vcme (<1000 km s^{-1})
	⩾0.30	2.0 E−4	3.88	Vcme (⩾1000 km s^{-1}) versus Vcme (<1000 km s^{-1})
Eastern	<0.31	1.7 E−1	1.38	No-CME versus $W < 360°$
	<0.31	4.1 E−2	2.08	$W < 360°$ versus $W = 360°$
	⩾0.31	1.7 E−1	1.40	No-CME versus $W < 360°$
	⩾0.31	1.1 E−3	3.42	$W < 360°$ versus $W = 360°$
Western	<0.30	1.0 E−2	2.63	No-CME versus $W < 360°$
	<0.30	5.9 E−4	3.56	$W < 360°$ versus $W = 360°$
	⩾0.30	5.3 E−2	1.97	No-CME versus $W < 360°$
	⩾0.30	8.2 E−2	1.76	$W < 360°$ versus $W = 360°$

Note.
[a] Format is: n E–$X = n \times 10^{-X}$.

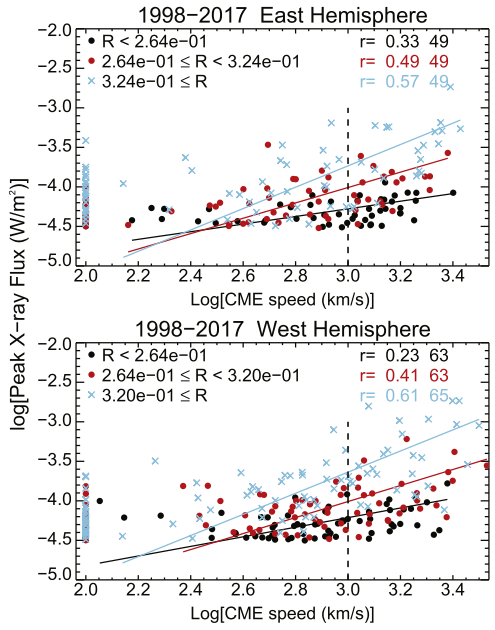

Figure 2. Log Fp vs. log CME speed Vcme for three groups of peak X-ray flux ratios R. X-ray flares with no associated CMEs are plotted at log CME speed = 2.0. Flares with associated CMEs are divided into three R groups of approximately equal sizes. Matching color-coded lines are geometric mean regression lines, with Pearson CCs r and numbers of CMEs indicated in the top right of each panel. Vertical dashed lines are placed at Vcme = 1000 km s^{-1}.

Figure 2 linear regression lines which are geometric means of the two linear regressions of log Fp versus log Vcme and of log Vcme versus log Fp, also known as the reduced major axis (Isobe et al. 1990).

Now we see in Figure 2 that CMEs of comparable Vcme values clearly sort associated flares similarly to the trend of Figure 1, with the largest flares (blue crosses) having the largest R values and the smallest flares (black dots) having the smallest R values. As R values are measures of flare temperatures, the flares associated with a given range of Vcme roughly range from large and hot to small and cool. The three R groups are all well separated, and the Pearson r CCs for each group, which are largest for the highest R group, are shown in the panels of Figure 2. That ranking of the r values could change if we had extended our flare threshold to include >M1 flares. Averages of the three CME-associated group numbers in the eastern and western hemisphere are 49 and 64 events, respectively, so all correlations of Figure 2 are significant at better than the 5% level (Bevington & Robinson 2003).

2.2. Peak-flux Ratios and CME Widths

In addition to speeds Vcme, CME widths W have been weakly correlated with SEP peak intensities (Kahler et al. 1999; Kahler & Reames 2003; Cane et al. 2010; Dierckxsens et al. 2015), and we look for a relation between the X-ray flare ratios R and associated CME W. Figure 3 show plots of W, again in the R–Fp format of Figure 1. We divided the CMEs into two groups of the many full halo ($W = 360°$) CMEs and those with $W < 360°$. As with CME speeds Vcme, we again get a separation of W groups in both hemispheres. The t-test parameters of the three populations are given in Table 1. The P values are slightly larger than those of the CME Vcme group comparisons of Figure 2, and the separations are more significant between the $W < 360°$ and $W = 360°$ groups than between the no CMEs and $W < 360°$ groups. The result is not surprising as halo CMEs are known to be much faster and more

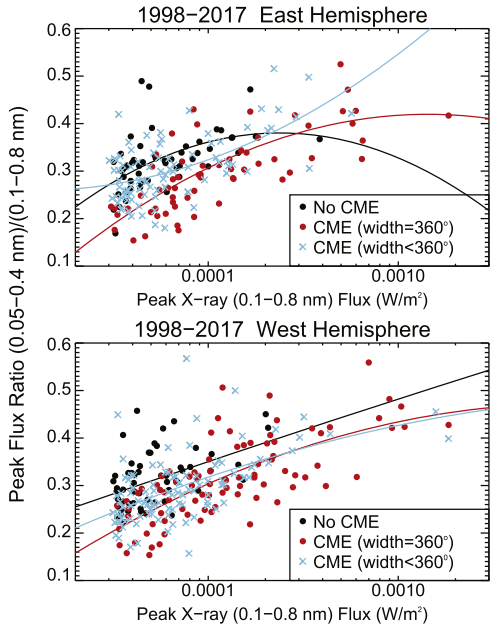

Figure 3. *R–Fp* plots for three classes of CME widths *W*. Solid lines are least-squares quadratic fits to color-matched symbols. Top panels: east hemisphere flares. Bottom panels: west hemisphere flares.

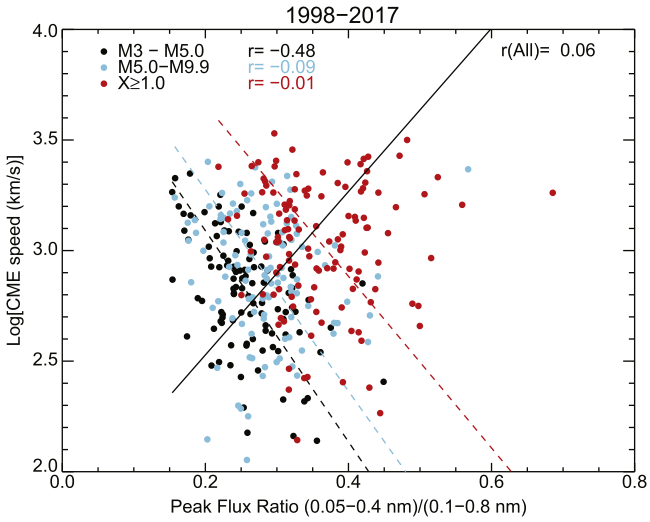

Figure 4. Log CME *V*cme vs. *R* for three groups of *Fp*. All CMEs from both hemispheres are plotted. Matching color-coded dashed lines are geometric mean regression lines of linear least-squares best fits, with Pearson CCs *r* indicated in the top.

energetic than ordinary CMEs (Gopalswamy et al. 2010). A plot of *W* versus *V*cme shows correlations for each range of *R*, but there is no significant separation among the *R* groups, and we do not include that plot here.

2.3. Peak-flux Ratios, CME Speeds, and Flare Sizes

Still unexplained by a simple conceptual model is why we find faster CMEs correlated with X-ray flares of lower *R*. To get a possibly better perspective on the relationship of *V*cme, *R*, and *Fp*, we show in Figure 4 a plot of log *V*cme for all CMEs versus *R* in which *Fp* values are color coded into three roughly equal size-bins. *Geometric means of* linear least-squares fits are indicated with dashed lines for each *Fp* group and by the solid line for the total group. For the M3.0–M5.0 flares we find definite negative correlations between *V*cme and *R*, while the signs of the slopes are more ambiguous for the M5.0–M9.9 and ⩾X1.0 flares.

3. Extreme Cases of Flares and CMEs

3.1. SEP Events with Erupting Filaments and Small (<M3.0) Flares

As reviewed above, fast CMEs producing gradual SEP events are usually accompanied by large solar X-ray flares, but there is a small class of moderately large gradual SEP events originating in large filament eruptions (FEs) accompanied by small (⩽M1.0) flares. Gopalswamy et al. (2015a) discussed four such FEs and reported five other large SEP events with C-class flares, two of which were determined to be FEs (Kahler et al. 2015). In a recent study Cliver et al. (2019) published a table of 8 FEs, now termed disappearing solar filaments (DSFs), associated with SEP events. Six of their 8 DSFs were associated with flares of size <M3.0. Combining the SEP events of Gopalswamy et al. (2015a) and Cliver et al. (2019), there are 11 events with associated flare sizes <M3.0, all of which are in the west hemisphere, as listed in Table 2. In the top panel of Figure 5 we add those 11 events to the updated version of the west hemisphere *R–Fp* plot of Figure 3 of KL18. The two >M3.0 flares of 2000 November 8 and 2001 November 22 of Table 2 are already included in Table 3. We do not include an extension of the many no-SEP flares to the C-class range for comparison, but it is clear that the separation of SEP and no-SEP flares by *R*, found originally in Garcia (1994, 2004) down to the M1.0 level, continues through the C-class range.

The goal of this section is to determine whether the low values of *R* for small X-ray flares with SEP events implies similarly low *R* values for fast CMEs that drive the SEP-associated shocks. The bottom panel of Figure 5 shows the distribution by *V*cme groups in the *R–Fp* format. A LASCO data gap occurred during the M2.7 flare of 1998 September 30, leaving 10 CMEs in the <M3.0 range, of which eight had *V*cme $\geqslant$ 1000 km s^{-1}. We find that the general relation of low *R* for fast CMEs shown in Figure 1 also holds down to the C-level range of flares, at least for the SEP-associated events.

3.2. Flare-rich and CME-poor Solar AR 12192

The decline of weak solar cycle 24 was punctuated by AR 12192, the largest AR since 1990 November (Thalmann et al. 2015), which crossed the solar disk in 2014 October 17 to 30. It was remarkable for its productivity of six X-class and at least 30 M-class flares, nearly all of which had no associated CMEs, in strong contradiction to earlier statistics of good CME associations with large flares (Yashiro et al. 2006; Yashiro & Gopalswamy 2008). To understand that lack of associated CMEs using magnetic field models and observations of those flares and their AR environment has been an ongoing goal of many investigator groups (e. g., Chen et al. 2015; Sun et al. 2015; Thalmann et al. 2015; Inoue et al. 2016; Jiang et al. 2016; Liu et al. 2016; Panesar et al. 2016; Zhang et al. 2017; Amari et al. 2018; Gopalswamy 2018; Green et al. 2018; Prasad et al. 2018; Li et al. 2018).

Our original NOAA list of ⩾M3.0 flares required solar locations to be included in the Table 3 and omitted several ⩾M3.0 flares in AR 12192. We have made location associations for all those flares and included them in the Table.

Table 2
X-ray Flares and CME Speeds of FE SEP Events

Date yyyy/mmm/dd	X-ray Peak (UT)	Flare Class	Solar Location	Author Refer[a]	SEP (pfu)	*V*cme (km s^{-1})
1998 Sep 30	13:50	M2.7	N19W85	C	1000	NA
2000 Apr 4	15:41	C9.7	N16W66	G, C, K	55	1188
2000 Sep 12	13:00	M1.0	S17W09	G	320	1550
2000 Oct 25	11:25	C4.0	N10W66	G	15	770
2000 Nov 8	23:28	M7.4	N10W75	C	4000	1738
2001 Nov 22	23:30	M9.9	S15W34	C	30	1437
2002 May 22	03:54	C5.0	S22W53	C, G	4	1557
2004 Apr 11	04:19	C9.6	S14W49	K, G	35	1645
2004 Jul 25	15:14	M1.1	N08W33	C	60	1333
2010 Aug 14	10:05	C4.4	N17W52	G	14	1205
2011 Nov 26	07:10	C1.2	N27W49	C, G	80	933
2012 Sep 27	23:57	C3.7	N06W34	G	28	1035
2013 Sep 29	23:39	C1.1	N15W29	C G	182	1179

Note.
[a] C, Table 2 of Cliver et al. (2019) G, Tables 1 and 4 of Gopalswamy et al. (2015a) K, Table 1 of Kahler et al. (2015).

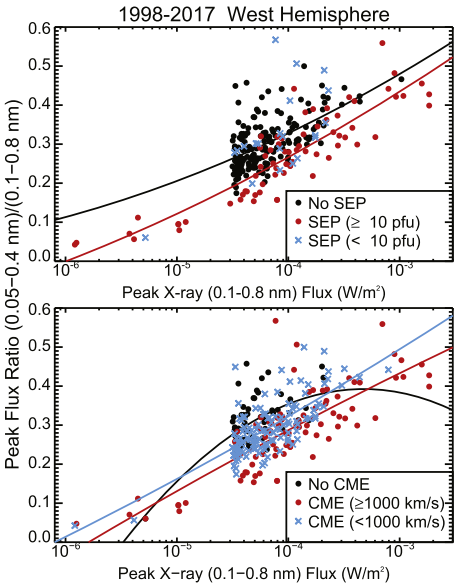

Figure 5. Extensions of *R–Fp* plots down to C1.0 flares to include the additional 11 west hemisphere SEP events of Table 2. Top: updated SEP events similar to lower left panel of Figure 1, in which the <10 pfu SEP events were treated as No-SEP events. Quadratic least-squares fits are shown for the no-SEP and ⩾10 pfu SEP events. Bottom: *R–Fp* plot of Figure 1 lower right panel extended to include EP CMEs of Table 2. Quadratic least-squares fits for each CME category are shown.

They can now be compared with the larger statistical distributions of CME occurrence and *V*cme we found in the previous section. Of the cited works above, only Chen et al. (2015) and Liu et al. (2016) provided tables listing all M and X flares of AR 12192 and their CME associations. Neither authors give their selection criteria for CME association, but they agree that only the M4.0 flare at 07:48 UT on October 24 had an associated CME, for which *V*cme = 677 km s^{-1}, the value given in the LASCO CDAW catalog (Gopalswamy et al. 2009) and the fclist.

Our Table 3 lists 16 flares in AR 12192, of which three have CME associations. Besides the M4.0 flare on October 24, we also give CME associations for the X1.1 flare on October 19 and the X3.1 on October 24, contrary to the above investigations. An alternative source of CME listings is the Computer Aided CME Tracking software (CACTus) catalog online at http://sidc.oma.be/cactus/catalog.php (Robbrecht & Berghmans 2004), which provides listings of automated detections of CMEs from the LASCO coronagraph. The M4.0 October 24 and X1.1 October 19 flares have associated CMEs #0098 and #0073 in the "Lasco quick-look CME" page of the CACTus catalog, but there is none for the X3.1 flare on October 24. Further work might be merited, in particular, for the X3.1 flare on October 24, the focus of three studies (Inoue et al. 2016; Jiang et al. 2016; Prasad et al. 2018), which occurred close enough to central meridian that an associated CME might be difficult to observe due to projection effects.

We show the *R–Fp* plot of the 16 AR 12192 flares in Figure 6 along with fast CMEs combined from both hemispheres and quadratic best fits to both populations. Note that the three AR 12192 CMEs discussed above have *V*cme < 1000 km s^{-1} and are not distinguished from the remaining non-CME flares. The basic result is that the AR 12192 flares lie well above the population with fast CMEs, as was the case with the non-CME flares of Table 3 shown in Figure 1. The AR 12192 flares do not differ from other large non-CME flares in terms of the *R–Fp* relationship and support the general conclusion that flares with no or slow CMEs are characterized by relatively higher X-ray peak temperatures than those with fast CMEs.

4. Discussion

In our earlier work (KL18) we updated the Garcia (1994, 2004) result showing that for a given X-ray flare *Fp*, SEP events were associated preferentially with lower ratios *R*, indicative of cooler X-ray flares (Figure 1). We speculated that the physical reason for this result was that cooler flares were associated with the faster CMEs required to drive the shocks producing SEP events. Starting with our modified and updated list of ⩾M3.0 flares, we searched the CDAW list for LASCO CMEs well associated in time and location with the flares and then resolved all association differences with the fclist.

Unlike the SEP event associations with a bias for western hemisphere flare sources, the CME associations in each hemisphere should be similar and provide a consistency check on any single hemisphere result. First, we find (Figure 1) that

Table 3
X-ray Flares > M3 and Associated CMEs and SEP Events

Date yyyy/mmm/dd	X-ray Peak	Flare Class	Solar Location	Peak X-ray Ratio	CME Speed	CME Width	SEP Date/ Onset U	SEP *Ip*
1998 Apr 27	9:20	X 1.0	S16E50	2.32E−01	1385	360	⋯	⋯
1998 Apr 29	16:37	M 6.8	S18E20	1.85E−01	1374	360	29/2100	1.4
1998 May 2	13:42	X 1.1	S15W15	2.85E−01	938	360	2/1400	150
1998 May 6	8:09	X 2.7	S11W65	3.73E−01	1099	190	6/0800	210
1998 May 9	3:40	M 7.7	S11W90	5.67E−01	2331	178	9/0500	9
1998 May 10	13:20	M 3.9	S29E88	2.64E−01	None	None	⋯	⋯
1998 Nov 5	19:55	M 8.4	N22W18	3.20E−01	1118	360	5/2200	7
1998 Nov 24	2:20	X 1.0	S30W90	5.06E−01	1798	360	24/0300	1.5
1998 Nov 28	5:52	X 3.3	N17E32	3.06E−01	495	88	⋯	⋯
1998 Dec 17	7:45	M 3.2	S27W46	2.09E−01	302	360	⋯	⋯
1999 Feb 28	16:39	M 6.6	N28W06	2.62E−01	329	64	⋯	⋯
1999 Mar 16	21:41	M 6.2	N23W39	3.07E−01	None	None	⋯	⋯
1999 Mar 17	9:56	M 3.2	N23W44	2.66E−01	None	None	⋯	⋯
1999 Apr 3	23:10	M 4.3	N29E81	2.06E−01	923	156	⋯	⋯
1999 Apr 4	5:25	M 5.4	N18E72	1.87E−01	1203	173	⋯	⋯
1999 May 3	6:02	M 4.4	N15E32	1.63E−01	1584	360	3/1800	2
1999 May 7	4:41	M 3.2	N20E87	2.66E−01	398	13	⋯	⋯
1999 May 8	14:40	M 4.6	N23W75	2.40E−01	641	125	⋯	⋯
1999 May 9	18:07	M 7.6	N26W90	2.89E−01	615	172	9/1900	1.7
1999 Jun 4	7:03	M 3.9	N17W69	1.79E−01	2230	150	4/0800	64
1999 Jul 16	15:50	M 3.1	N43W71	2.39E−01	746	111	⋯	⋯
1999 Jul 19	8:46	M 5.8	N18E59	1.80E−01	719	102	⋯	⋯
1999 Jul 24	8:02	M 3.3	S28E78	2.19E−01	313	57	⋯	⋯
1999 Jul 27	14:05	M 3.0	N23W50	1.95E−01	592	72	⋯	⋯
1999 Jul 29	19:36	M 5.1	N25E51	2.46E−01	199	24	⋯	⋯
1999 Feb 2	21:25	X 1.4	S18W46	3.17E−01	292	157	⋯	⋯
1999 Feb 4	5:57	M 6.0	S16W64	3.17E−01	405	144	⋯	⋯
1999 Feb 20	23:08	M 9.8	S25E64	3.59E−01	812	76	⋯	⋯
1999 Feb 21	16:34	M 3.7	S25E56	2.68E−01	841	68	⋯	⋯
1999 Feb 21	22:14	M 5.9	S24E52	3.27E−01	1295	66	⋯	⋯
1999 Feb 25	1:36	M 3.6	S28E21	2.54E−01	195	17	⋯	⋯
1999 Feb 27	13:07	M 5.5	S23W09	2.67E−01	None	None	⋯	⋯
1999 Feb 27	16:36	M 3.0	S31E04	1.69E−01	None	None	⋯	⋯
1999 Feb 28	18:05	X 1.1	S26W14	3.02E−01	462	245	⋯	⋯
1999 Oct 14	9:00	X 1.8	N11E32	3.16E−01	1250	360	⋯	⋯
1999 Nov 16	2:46	M 3.8	N17E38	2.40E−01	636	98	⋯	⋯
1999 Nov 16	4:10	M 3.0	N12W74	2.33E−01	None	None	⋯	⋯
1999 Nov 24	23:37	M 3.0	S19W43	4.49E−01	255	87	⋯	⋯
1999 Nov 26	13:43	M 6.0	S15W59	2.50E−01	193	64	⋯	⋯
1999 Nov 27	12:12	X 1.4	S15W68	3.17E−01	235	68	⋯	⋯
1999 Dec 22	19:04	M 5.3	N24E19	2.61E−01	605	360	⋯	⋯
1999 Dec 28	0:48	M 4.5	N20W56	2.39E−01	672	82	⋯	⋯

(This table is available in its entirety in machine-readable form.)

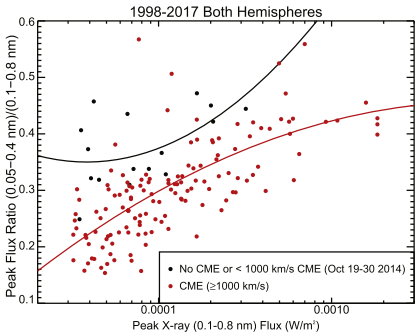

Figure 6. *R–Fp* plot comparing two populations. Black dots are the 16 flares of AR 12192 with quadratic least-squares best fit, and red dots are all X-ray flares with associated *V*cme $\geqslant$ 1000 km s^{-1} CMEs, which are the combined events of both hemispheres of Figure 1.

flares of a given *Fp* without CMEs are somewhat hotter (higher *R*) than those with slow (*V*cme $<$ 1000 km s^{-1}) CMEs. This result was found earlier by Kay et al. (2003) with a smaller data set of 69 flares. They speculated that the occurrence of a CME means that less energy goes into heating the associated flare. Perhaps consistent with that view, we find a more significant separation in bins of *R* (Table 1) between the groups of slow (*V*cme $<$ 1000 km s^{-1}) and fast (*V*cme $\geqslant$ 1000 km s^{-1}) CMEs, where the latter group are known to have higher associations with SEP events. We further explored the role of ratios *R* in the general correlation between X-ray *Fp* and associated *V*cme. The result (Figure 2) is that within the correlation there are strong separations (Table 1) by *R*, showing that within a given range of CME speeds the associated cooler (lower *R*) flares have lower peak X-ray fluxes and the hotter have higher peak X-ray fluxes. This effect is more clearly shown in Figure 4.

In KL18 we pointed out that a comprehensive analysis of 399 M and X *GOES* flares by Aschwanden (2017) found a scaling law of $V\mathrm{cme} \sim T_e^{0.5}$, based on an assumed equipartition between CME kinetic energy and flare thermal energy. That result is consistent with earlier (Yashiro & Gopalswamy 2008) statistical log correlations found between CME *V*cme and X-ray *Fp* ($r = 0.50$) and between CME kinetic energy and X-ray *Fp* ($r = 0.48$). Results showing consistent ratios of CME energies to dissipated magnetic energies (Gopalswamy et al. 2015b; Aschwanden 2016) also support the equipartition argument. Figure 8(a) of Aschwanden (2017) appears inconsistent with both our Figure 1 and the Kay et al. (2003) explanation that CME activity removes energy from the source region, resulting in less energy available for flares, as indicated by lower peak flare temperatures. Figure 4 may help to resolve this observational paradox. In accordance with Aschwanden (2017), there is a very weak correlation between *V*cme and *R*, indicated by the linear best-fit solid line. However, if we consider only specific ranges of selected *Fp*, shown by the three color-coded groups, then we find slightly negative correlations between *V*cme and *R*, as expected in the scheme of Kay et al. (2003). Thus, the validity of each energy scaling concept may depend on whether *Fp* is held constant or allowed to be a free parameter.

Our inputs to the Figure 4 plots have significant differences from those of Figure 8(a) of Aschwanden (2017). Our *V*cme values are straight from the LASCO catalog, and *R* is based on the two soft X-ray bands of the *GOES* XRS, while Aschwanden (2017) modeled a CME speed combining LASCO observations with a gravitational deceleration term and computed an emission measure-weighted flare temperature T_w using Atmospheric Imaging Assembly/*Solar Dynamics Observatory* data. Further, Kay et al. (2003) compared only two groups of flares with and without CMEs, and their summary Table 1 showed an overall higher mean temperature for flares with CMEs. Our result provides input for, but does not support, a simple model for energy scaling between flares and associated CMEs (Vršnak 2016).

In Section 3 we extended the *R*–*Fp* analysis to two extreme groups of X-ray flares, first, the large M and X-class flares of AR 12192, spectacular in their general lack of CME associations, and second, the very small (<M3.0) flares which occurred with EFs and associated SEP events. Both groups were found to fit well into the *R*–*Fp* plots. The AR 12192 flares had large values of *R*, expected for flares lacking CME associations (Figure 6), and the small FE flares had low values of *R*, associated with the expected fast CMEs needed to produce SEP events (Figure 5). These extreme X-ray flares show that the original T_e versus *Fp* plots of Garcia (1994, 2004) for selecting SEP events are very inclusive of all X-ray flares and reveal a fundamental relationship between cooler flare temperatures and faster CMEs (Figures 2 and 4).

Although CME speeds are considered the primary factor in driving shocks that produce SEP events, the associated widths *W* must also play a factor in the geometry and locations of CMEs and have been determined statistically to be one factor in SEP production. We did a similar *R*–*Fp* comparison to look for any sorting of CME widths, where we used values from the LASCO CDAW listings. The limitations of plane-of-sky observations, especially the halo events, are well known, so we did not expect strong separation of the CME widths in the *R*–*Fp* plots. However, the result is surprisingly similar to that obtained for *V*cme in terms of the separations of halo and non-halo *W* groups (Table 1). A possible interpretation is that the relatively poorer correlations between SEP event peak intensities and CME *W* may be due to a worse characterization of *W* than of *V*cme when using the CDAW CME values. Considerable work has been done on modeling CME speeds and widths using coronagraph images from the *STEREO* A and B spacecraft (e.g., Park et al. 2017; Balmaceda et al. 2018; Pluta et al. 2019). It may be worthwhile to repeat the work here using modeled CME parameters in which *V*cme and *W* based on *STEREO* observations are the input parameters.

As another parametric consideration, KL19b looked at X-ray flare time durations ΔT. They used the readily available SWPC definition of time from onset to half peak flux, less desirable than end times of near background (Veronig et al. 2002; Ryan et al. 2016; Kawabata et al. 2018). A direct comparison of flare log ΔT versus log *V*cme shows very significant positive correlations, which are independent of flare class. To complete the statistical comparison among ΔT, *V*cme, and *R*, KL19b find (their Figure 3) modest inverse correlations between ΔT and *R*, where the separation between M and X flares shows the well known (e.g., Ryan et al. 2012) trend toward larger *R* values for larger peak flare fluxes. We can conclude not only that SEP events are associated with faster ($V\mathrm{cme} \geqslant 1000\,\mathrm{km\,s^{-1}}$) and wider CMEs, but that the associated X-ray flares have lower peak temperatures (smaller *R*) and longer ΔT (Cane et al. 2010) than non-SEP events.

5. Conclusions

The basic question addressed in this work is whether the correlation of SEP events with X-ray flares of lower *R* can be attributed to a similar correlation of faster CMEs with flares of lower *R*. The answer is clearly yes, and we further found that X-ray flare ratios *R* serve to spread the correlation between *Fp* and *V*cme into bands from low *R* and low *Fp* to high *R* and high *Fp* for any range of *V*cme (Figure 2). Finally, we find that flares with low *R* are also correlated with larger CME *W*, where we have distinguished only the halo from non-halo CMEs.

S.K. was funded by AFOSR Task 18RVCOR122. A.L. was supported by AFRL contract FA9453-15-C-0050. We thank the reviewer for pointing out the fclist catalog and for recommendations that improved the manuscript. CME data were taken from the CDAW LASCO catalog. This CME catalog is generated and maintained at the CDAW Data Center by NASA and The Catholic University of America in cooperation with the Naval Research Laboratory. *SOHO* is a project of international cooperation between ESA and NASA. This work was (partly) carried out by using Hinode Flare Catalog (https://hinode.isee.nagoya-u.ac.jp/flare_catalogue/), which is maintained by ISAS/JAXA and Institute for Space-Earth Environmental Research (ISEE), Nagoya University.

ORCID iDs

A. G. Ling https://orcid.org/0000-0002-8768-1819
S. W. Kahler https://orcid.org/0000-0002-0470-7236

References

Amari, T., Canou, A., Aly, J.-J., Delyon, F., & Alauzet, F. 2018, Natur, 554, 211
Aschwanden, M. J. 2016, ApJ, 831, 105
Aschwanden, M. J. 2017, ApJ, 847, 27
Balch, C. C. 2008, SpWea, 6, S01001

Balmaceda, L. A., Vourlidas, A., Stenborg, G., & Dal Lago, A. 2018, ApJ, 863, 57
Belov, A. 2009, AdSpR, 43, 467
Belov, A. V. 2017, Ge&Ae, 57, 727
Bevington, P. R., & Robinson, D. K. 2003, Data Reduction and Error Analysis for the Physical Sciences (New York: McGraw-Hill)
Cane, H. V., Richardson, I. G., & von Rosenvinge, T. T. 2010, JGR, 115, A08101
Chen, H., Zhang, J., Ma, S., et al. 2015, ApJL, 808, L24
Cliver, E. W., Kahler, S. W., Kazachenko, M., & Shimojo, M. 2019, ApJ, 877, 11
Desai, M., & Giacalone, J. 2016, LRSP, 13, 3
Dierckxsens, M., Tziotziou, K., Dalla, S., et al. 2015, SoPh, 290, 841
Garcia, H. A. 1994, ApJ, 420, 422
Garcia, H. A. 2004, SpWea, 2, S02002
Gopalswamy, N. 2018, in Extreme Events in Geospace, 1st ed., Origins, Predictability, and Consequences, ed. N. Buzulukova (Amsterdam: Elsevier), 37
Gopalswamy, N., Mäkelä, P., Akiyama, S., et al. 2015a, ApJ, 806, 8
Gopalswamy, N., Yashiro, S., & Akiyama, S. 2015b, ApJ, 809, 106
Gopalswamy, N., Yashiro, S., Michalek, G., et al. 2009, EM&P, 104, 295
Gopalswamy, N., Yashiro, S., Michalek, G., et al. 2010, SunGe, 5, 7
Green, L. M., Török, T., Vršnak, B., Manchester, W., IV, & Veronig, A. 2018, SSRv, 214, 46
Inoue, S., Hayashi, K., & Kusano, K. 2016, ApJ, 818, 168
Isobe, T., Feigelson, E. D., Akritas, M. G., & Babu, G. J. 1990, ApJ, 364, 104
Jiang, C., Wu, S. T., Yurchyshyn, V., et al. 2016, ApJ, 828, 62
Kahler, S., Gopalswamy, N., Makela, P., Akiyama, S., & Yashiro 2015, ICRC (The Hague), 34, 48
Kahler, S. W., Burkepile, J., & Reames, D. 1999, ICRC (Salt Lake City, UT), 6, 248
Kahler, S. W., & Ling, A. G. 2018, JSWSC, 8, A47
Kahler, S. W., & Ling, A. G. 2019a, ApJ, 872, 89
Kahler, S. W., & Ling, A. G. 2019b, ICRC (Madison, WI), 1089, 36
Kahler, S. W., & Reames, D. V. 2003, ApJ, 584, 1063
Kahler, S. W., White, S. M., & Ling, A. G. 2017, JSWSC, 7, A27
Kawabata, Y., Iida, Y., Doi, T., et al. 2018, ApJ, 869, 99
Kay, H. R. M., Harra, L. K., Matthews, S. A., Culhane, J. L., & Green, L. M. 2003, A&A, 400, 779
Li, T., Hou, Y., Yang, S., & Zhang, J. 2018, ApJ, 869, 172
Liu, L., Wang, Y., Wang, J., et al. 2016, ApJ, 826, 119
Miteva, R., Klein, K.-L., Malandraki, O., & Dorrian, G. 2013, SoPh, 282 579
Nuñez, M. 2018, JSWSC, 8, A36
Panesar, N. K., Sterling, A. C., & Moore, R. L. 2016, ApJL, 801, L23
Park, J., & Moon, Y.-J. 2014, JGR, 119, 9456
Park, J., Moon, Y.-J., & Lee, H. 2017, ApJ, 844, 17
Pluta, A., Mrotzek, N., Vourlidas, A., Bothmer, V., & Savani, N. 2019, A&A, 623, A139
Prasad, A., Bhattacharyya, R., Hu, Q., Kumar, S., & Nayak, S. S. 2018, ApJ, 860, 96
Reames, D. V. 2013, SSRv, 175, 53
Reames, D. V. 2017, Lecture Notes in Physics, Vol. 932, Solar Energetic Particles: A Modern Primer on Understanding Sources (Berlin: Springer)
Reames, D. V. 2018, SSRv, 214, 61
Robbrecht, E., & Berghmans, D. 2004, A&A, 425, 1097
Ryan, D. F., Dominique, M., Seaton, D., Stegen, K., & White, A. 2016, A&A, 592, A133
Ryan, D. F., Milligan, R. O., Gallagher, P. T., et al. 2012, ApJS, 202, 11
Salas-Matamoros, C., & Klein, K.-L. 2015, SoPh, 290, 1337
Sun, X., Bobra, M. G., Hoeksema, J. T., et al. 2015, ApJL, 850, L43
Takahashi, T., Mizuno, Y., & Shibata, K. 2016, ApJL, 833, L8
Thalmann, J. K., Su, Y., Temmer, M., & Veronig, A. M. 2015, ApJL, 801, L23
Trottet, G., Samwel, S., Klein, K.-L., Dudok de Wit, T., & Miteva, R. 2015, SoPh, 290, 819
Valtonen, E., & Ameri, D. 2015, ICRC (The Hague), 34, 87
Veronig, A., Temmer, M., Hanslmeier, A., Otruba, W., & Messerotti, M. 2002, A&A, 382, 1070
Vršnak, B. 2016, AN, 337, 1002
Wilks, D. S. 2006, Statistical Methods in the Atmospheric Sciences (Amsterdam: Elsevier), 138
Yashiro, S., Akiyama, S., Gopalswamy, N., & Howard, R. A. 2006, ApJL, 650, L143
Yashiro, S., & Gopalswamy, N. 2008, in IAU Symp. 257, Universal Heliophysical Processes, ed. N. Gopalswamy & D. F. Webb (Cambridge: Cambridge Univ. Press), 233
Yashiro, S., Michalek, G., & Gopalswamy, N. 2008, AnGeo, 26, 3103
Zhang, J., Li, T., & Chen, H. 2017, ApJ, 845, 54